Prescribed-Time Safety Filter for a 7-DOF Robot Manipulator: Experiment and Design

Alexander Bertino[®], Peiman Naseradinmousavi[®], and Miroslav Krstić[®], Fellow, IEEE

Abstract—In this research effort, we formulate a prescribedtime safety filter (PTSf) for the case of a redundant manipulator performing a fixed-duration task. This formulation, which is based on a quadratic programming approach, yields a filter that is capable of avoiding multiple obstacles in a minimally invasive manner with bounded joint torques, while simultaneously allowing the nominal controller to converge to positions located on the boundary of the safe set by the end of the fixed-duration task. To demonstrate the efficacy of the proposed method, we performed a series of simulations and experiments on Baxter, a seven-DOF collaborative robot manipulator. In these simulations and experiments, Baxter must follow a 6-s parabolic trajectory as closely as possible while navigating around a large spherical obstacle blocking its path and place an object precisely on the surface of a table without overshoot by the end of the 6 s. The results of our simulations and experiments demonstrated the ability of the PTSf to enforce safety throughout the 6-s task, while allowing the robot manipulator to make contact with the table and thus achieve the desired goal position by the end of the task. Furthermore, when compared with the exponential safety filter (ESf), which is the state-of-the-art in current literature, our proposed method yielded consistently lower joint jerks. Thus, for tasks with a fixed duration, the proposed PTSf offers performance benefits over the exponential filters currently present in literature.

Index Terms—Control, prescribed-time safety filter (PTSf), robotics.

I. INTRODUCTION

S THE usage of robot manipulators in collaborative environments has dramatically risen in recent years, ensuring that a robot manipulator is able to operate safely has become an important goal for modern control systems [11], [19], [24], [26], [48]. In this context, safety refers to the ability of a robot manipulator to avoid dangerous collisions, both with humans and other potential obstacles. To ensure safety

Manuscript received 28 April 2022; revised 23 November 2022; accepted 1 February 2023. This work was supported by the National Science Foundation under Award 1823951-1823983. Recommended by Associate Editor A. Macchelli. (Corresponding author: Alexander Bertino.)

Alexander Bertino is with the Department of Mechanical Engineering, San Diego State University, San Diego, CA 92115 USA, and also with the Department of Mechanical and Aerospace Engineering, University of California San Diego, La Jolla, CA 92093 USA (e-mail: abertino6245@sdsu.edu).

Peiman Naseradinmousavi is with the Department of Mechanical Engineering, San Diego State University, San Diego, CA 92115 USA (e-mail: pnaseradinmousavi@sdsu.edu).

Miroslav Krstić is with the Department of Mechanical and Aerospace Engineering, University of California San Diego, La Jolla, CA 92093 USA (e-mail: krstic@ucsd.edu).

Color versions of one or more figures in this article are available at https://doi.org/10.1109/TCST.2023.3243403.

Digital Object Identifier 10.1109/TCST.2023.3243403

during the operation of a collaborative robot manipulator, safety must be considered at every level of the design and operation of the manipulator. From a mechanical perspective, collaborative robot manipulators should be designed to be compliant, so that potential collisions are less damaging. From a planning perspective, the reference trajectories generated for collaborative robot manipulators should be designed to avoid collisions with obstacles. From a controls' perspective, preventative torques should be applied to the manipulator whenever necessary to avoid collisions with obstacles. In this article, we focus our efforts toward this controls' perspective, and thus on the design of control torques that ensure the robot manipulator remains within a user-defined safe set.

In the past several years, a large amount of research has been devoted toward the design of control barrier functions (CBFs) for robot manipulators [2], [10], [22], [23], [25], [28], [29], [30], [35], [37], [40], [41], [43], [47], [50], [55], [57]. CBFs function as a safety filter for a potentially unsafe nominal controller, overriding the nominal control torques when the boundary of the safe set is approached faster than a designed convergence rate. Typically, this override torque is determined via a quadratic program minimizing the difference between the nominal and override torques, and thus CBFs can be characterized as minimally invasive. The majority of CBFs formulated for robot manipulators are based on the concept of exponential safety filters (ESfs), which were first introduced by Nguyen and Sreenath [45]. Using this method, the maximum rate of convergence to the boundary of the safe set is limited to be exponential, and consequently the robot manipulator can approach but will never reach the boundary of the safe set.

While ESfs are designed to be minimally invasive, their presence can interfere with the operation of set-duration tasks when the goal position of the end-effector is located near the boundary of the safe set. For an example of such a scenario, one could consider a robot that brings a glass of water to a patient's mouth without risking the injury of the patient's teeth. Under ideal conditions such as zero initial tracking error, a trajectory-tracking nominal controller operating in such a scenario would converge to the desired goal position within a fixed time that is governed by the design of the trajectory. However, when an ESf is applied to this nominal controller, the rate of approach to the goal position, which lies on the boundary of the safe set, is limited to be exponential. Thus, the manipulator will not reach the desired goal position by the fixed time and will instead be located near the desired goal position. After an additional period of time governed by the

 $1063-6536 \ @\ 2023\ IEEE.\ Personal\ use\ is\ permitted,\ but\ republication/redistribution\ requires\ IEEE\ permission.$ See https://www.ieee.org/publications/rights/index.html for more information.

conservativeness of the ESf, the tracking error will become negligible. Thus, in this circumstance, the ESf has destroyed the prescribed-time convergence property of the nominal controller and introduced uncertainty into the system as to when the tracking error will become negligible. In circumstances such as the provided example, the additional duration of the task may not be a significant detriment, as the delay in the patient receiving water is unlikely to be life-threatening. However, there are numerous cases in which both safety and timing are critical factors, and thus the limiting behavior of the ESf is undesirable. Consider instead a robot manipulator that is assisting with the surgery of a patient. In this case, safety is desired to not further injure the patient or doctors, but timeliness is also critical to preserve the life of the patient. To address the time-critical aspect of scenarios such as these, a considerable amount of research has been devoted toward the development of control methods for robot manipulators which are capable of guaranteeing an upper bound on the convergence time, achieving convergence of tracking errors to zero within a finite period of time [12], [20], [21], [27], [31], [32], [33], [34], [36], [38], [39], [42], [44], [46], [49], [51], [52], [53], [54], [56], [58], [59], [60], [61], [62]. When the nominal controller is capable of ensuring convergence within a finite time, enforcing a condition of exponential convergence to the boundary of the safe set is counterproductive.

Using concepts from prescribed-time stabilization [51], in which convergence to the desired setpoint is achieved in a time explicitly prescribed as a controller parameter, Abel et al. [1] have recently developed a prescribed-time safety filter (PTSf) for a chain of integrators. Rather than enforcing safety for an indefinite period of time, the PTSf enforces safety only for a finite period of time that is explicitly set as a filter parameter T. Notably, this procedure allows the nominal controller to reach the boundary of the safe set by the end of the prescribed duration T. If the boundary of the safe set is approached in this manner, all the temporal derivatives of the system state will approach 0 as $t \to T$, meaning the convergence to the barrier will be infinitely soft. To achieve this beneficial property, a scaling of the filter gains by a function of time that grows unbounded toward the terminal time is used. This approach can be interpreted as a safety filter that becomes less strict as the terminal time is approached, allowing the nominal controller to converge to states that are nearby or even located on the boundary of the safe set.

In this research effort, we reformulate the PTSf initially proposed by Abel et al. [1] for the case of a redundant manipulator performing a fixed-duration task. This formulation yields a filter that is capable of avoiding multiple obstacles in a minimally invasive manner with bounded joint torques, while simultaneously allowing the nominal controller to converge to positions located on the boundary of the safe set by the end of the fixed-duration task. Compared with the formulation proposed in [1], our proposed method has the advantage of being capable of handling systems with multiple inputs, as well as systems with multiple obstacles that must be avoided. In addition, it is important to note that while the prescribed-time control of robot manipulators has

been addressed in manuscripts such as [18] and [51], this article is the first to address the design and experiment of a PTSf for robot manipulators. To demonstrate the efficacy of the proposed method, we perform a series of simulations and experiments on Baxter, a seven-DOF collaborative robot manipulator. In these simulations and experiments, Baxter must follow a 6-s parabolic trajectory as closely as possible while navigating around a large spherical obstacle blocking its path and place an object precisely on the surface of a table without overshoot by the end of the 6 s. To highlight the ability of this method to allow convergence to the barrier within a finite period of time, the nominal controller used in both the simulation and experiment is a prescribed-time controller which we previously formulated in [18]. The results of our simulations and experiments demonstrate the ability of the PTSf to enforce safety throughout the 6-s task, while allowing the robot manipulator to make contact with the table and thus achieve the desired goal position by the end of the task. Furthermore, we compare the performance of the PTSf method presented here to an ESf with a high gain, as well as an ESf with a low gain. When performed on the same task, the ESf with a high gain is able to make contact with the table within the 6-s task, but exhibits a much higher jerk in the joint torques than the PTSf in the beginning of the task. Conversely, the ESf with a low gain exhibits similar jerk values to the PTSf in the beginning of the task, but is not able to make contact with the table within the 6-s task. Thus, the PTSf proposed here outperforms the ESf when applied to fixed-duration tasks.

The organization of this article is as follows. In Section II, we present a brief overview of the dynamics of Baxter's right manipulator. In Section III, we present the design of the PTSf. In Section IV, we mathematically verify the ability of the PTSf to enforce the invariance of the safe set, as well as the feasibility of the proposed filter and boundedness of the filter torques when safety is enforced. In Section V, we present the results of the simulations and experiments performed on Baxter. Finally, in Section VI, we present the case that for tasks with a fixed duration, the proposed PTSf offers performance benefits over the exponential filters currently present in literature.

II. MATHEMATICAL MODELING

The redundant manipulator, which is being studied here, has seven DOFs as shown in Figs. 1 and 2. Baxter manipulator's Denavit–Hartenberg parameters are shown in Table I provided by the manufacturer. The Euler–Lagrange formulation leads to a set of seven coupled nonlinear second-order ordinary differential equations

$$M(q)\ddot{q} + C(q, \dot{q})\dot{q} + G(q) + F(\dot{q}) = \tau \tag{1}$$

where $q, \dot{q}, \ddot{q} \in \mathbb{R}^7$ are the angles, angular velocities, and angular accelerations of joints, respectively, and $\tau \in \mathbb{R}^7$ indicates the vector of joints' driving torques. Also, $M(q) \in \mathbb{R}^{7 \times 7}$ is a symmetric mass-inertia matrix, $C(q, \dot{q}) \in \mathbb{R}^{7 \times 7}$ is a matrix of Coriolis coefficients, $G(q) \in \mathbb{R}^7$ is a vector of gravitational loading, and $F(\dot{q}) \in \mathbb{R}^7$ represents a vector of frictional torques.



Fig. 1. Seven-DOF Baxter's arm at DSCL.

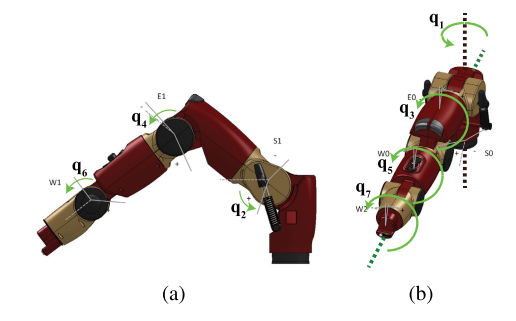


Fig. 2. Joints' configuration. (a) Sagittal view. (b) Top view.

TABLE I
BAXTER'S DENAVIT–HARTENBERG PARAMETERS

Link	a_i	d_i	α_i	q_i
1	0.069	0.27035	$-\pi/2$	q_1
2	0	0	$\pi/2$	$q_2 + \pi/2$
3	0.069	0.36435	$-\pi/2$	q_3
4	0	0	$\pi/2$	q_4
5	0.010	0.37429	$-\pi/2$	q_5
6	0	0	$\pi/2$	q_6
7	0	0.3945	0	q_7

Our verified coupled nonlinear dynamic model of the robot [3], [4], [5], [6], [7], [8], [9], [13], [14], [15], [16], [17] is used as the basis of the PTSf approach.

III. PTSF FOR ROBOT MANIPULATORS

We consider the following state-space representation of (1):

$$\dot{Q} = \begin{bmatrix} \dot{Q}_1 \\ \dot{Q}_2 \end{bmatrix} = \begin{bmatrix} Q_2 \\ \nu(t) \end{bmatrix} \tag{2}$$

in which we define

$$Q(t) = \begin{bmatrix} Q_1(t) \\ Q_2(t) \end{bmatrix} = \begin{bmatrix} q(t) \\ \dot{q}(t) \end{bmatrix}$$
 (3)

$$v(t) = \ddot{q}(t) = M^{-1}(q) \left(\tau(t) - C(q, \dot{q}) \dot{q}(t) - G(q) - F(\dot{q}) \right). \tag{A}$$

The purpose of the proposed PTSF is to ensure that Baxter's end-effector remains within the following user-defined safe set for the duration of the task:

$$\mathcal{H}_p = \left\{ p \in \mathbb{R}^3 | h_i(p) \ge 0, i = 1, \dots, m \right\}$$
 (5)

where

$$\frac{\partial^2 h_i}{\partial n^2} \ge 0 \quad \forall p \in \mathbb{R}^3, \quad i = 1, \dots, m$$
 (6)

and $p(q) \in \mathbb{R}^3$ is the position of the end-effector in the Cartesian coordinates, which is a function of the joint angles q. Thus, we can redefine this safe set in terms of Baxter's joint angles

$$\mathcal{H} = \{ q \in \mathbb{R}^7 | h_i(p(q)) \ge 0, i = 1, \dots, m \}.$$
 (7)

In this formulation, the robot manipulator must prevent collision between m obstacles, which each has a corresponding CBF h_i . As a consequence of (6), each of these obstacles must be convex. This barrier is positive when there is no collision, 0 when the robot manipulator and the obstacle make contact, and negative when the robot manipulator is within the barrier. Thus, ensuring the joint positions of Baxter are kept within the defined safe set (7) is equivalent to preventing a collision between the end-effector and an obstacle. The goal of the PTSf is formally defined as follows:

$$q(t) \in \mathcal{H} \quad \forall t \in [0, T)$$
 (8)

where T > 0 is the user-defined duration of the prescribedtime task, as well as the duration of enforcement of the PTSf.

To allow the robot manipulator to make contact with the barrier at time T, we use a scaling of the PTSf gains by a function of time that grows unbounded toward the time T

$$\mu_k(t) = \left(\frac{T}{T-t}\right)^k, \quad t \in [0, T), \quad k \in \mathbb{N}. \tag{9}$$

Note that the temporal derivative of this function can be computed as

$$\dot{\mu}_k(t) = \frac{k}{T} \mu_{k+1}(t), \quad t \in [0, T), \quad k \in \mathbb{N}.$$
 (10)

Due to the relative degree of the CBFs h_i being greater than 1, we pursue a backstepping design to enforce the invariance of (8). To this end, we define the following output functions:

$$y_{i1}(t) = h_i(p(q(t)))$$
 (11)

$$y_{i2}(t) = \frac{\partial h_i(p(q(t)))}{\partial q}\dot{q}(t) + c\mu_2(t)y_{i1}(t)$$
 (12)

where $y_{i1}(t)$, $y_{i2}(t) \in \mathbb{R}$ and $c \in \mathbb{R}$ is a design parameter to be determined. In this formulation, if we ensure that y_{i1} and y_{i2} are initially positive and remain positive for the duration of the prescribed-time task, the condition (8) will also be satisfied. In order for $y_{i1}(0) > 0$, the system must initially be safe. In order for $y_{i2}(0) > 0$, we must choose

$$c > \max \left\{ 0, -\frac{\frac{\partial y_{i1}(0)}{\partial q} \dot{q}(0)}{y_{i1}(0)} \right\}.$$
 (13)

To ensure that y_{i1} and y_{i2} remain positive in the interval $t \in [0, T)$, it is necessary to examine their underlying dynamics

$$\dot{y}_{i1} = -c\mu_2 y_{i1} + y_{i2} \tag{14}$$

$$\dot{y}_{i2} = \frac{2}{T}c\mu_3 y_{i1} + c\mu_2 \frac{\partial y_{i1}}{\partial q} \dot{q} + \dot{q}^{\top} \frac{\partial^2 y_{i1}}{\partial q^2} \dot{q} + \frac{\partial y_{i1}}{\partial q} \nu$$
 (15)

where (14) is obtained from rearranging (12), and (15) is obtained from taking the temporal derivative of (12) and applying (10). To enforce the positivity of h_1 and h_2 for

 $t \in [0, T)$, we permit only v(t) such that the following condition is satisfied:

$$\dot{y}_{i2} + c\mu_2 y_{i2} \ge 0, \quad i = 1, \dots, m.$$
 (16)

In Section IV, we will show that this is a sufficient condition for the positivity of h_i over the duration $t \in [0, T)$.

Before presenting the design of the PTSf, we first reformulate (16) in terms of the CBFs h_i , as well as the joint angles q and joint velocities \dot{q} . To this end, we first obtain several derivatives of the CBFs with respect to the joint angles

$$\frac{\partial h_i}{\partial q} = \frac{\partial h_i}{\partial p} J(q) \tag{17}$$

$$\dot{q}^{\top} \frac{\partial^2 h_i}{\partial q^2} \dot{q} = \dot{q}^{\top} J^{\top}(q) \frac{\partial^2 h_i}{\partial p^2} J(q) \dot{q} + \frac{\partial h_i}{\partial p} \dot{J}(q) \dot{q}$$
 (18)

in which

$$J(q) = \frac{\partial p(q)}{\partial q} \tag{19}$$

$$\dot{J}(q) = \sum_{i=1}^{7} \frac{\partial J(q)}{\partial q_i} \dot{q}_i \tag{20}$$

where $J(q) \in \mathbb{R}^{3 \times 7}$ is the Jacobian of the end-effector. We make the following assumption of its structure.

Assumption 1: There exists a positive constant $\sigma_{lb} > 0$ such that the minimum singular value of the end-effector Jacobian J(q(t)) satisfies the following inequality:

$$\sigma_{\min}(J(q(t))) \ge \sigma_{\text{lb}} \quad \forall t \in [0, T).$$
 (21)

Then, we substitute (11), (12), (15), and (17)–(19) into (16) to obtain

$$b_i^{\top} v \ge a_i, \quad i = 1, \dots, m \tag{22}$$

where

$$a_{i} = -\dot{q}^{\top} J^{\top}(q) \frac{\partial^{2} h_{i}}{\partial p^{2}} J(q) \dot{q} - \frac{\partial h_{i}}{\partial p} \dot{J}(q) \dot{q}$$
$$-c\mu_{3} \left(\frac{2}{T} + c\mu_{1} \right) h_{i} - 2c\mu_{2} \frac{\partial h_{i}}{\partial p} J(q) \dot{q}$$
(23)

$$b_i^{\top} = \frac{\partial h_i}{\partial p} J(q). \tag{24}$$

To enforce safety for the prescribed duration T in a minimally invasive manner, we apply the PTSf, formulated as a quadratic program minimizing the difference in joint acceleration caused by the filtered and nominal control torque

$$\nu_{\text{safe}} = \underset{w \in \mathbb{R}^7}{\arg \min} \|w - \nu_{\text{nom}}\|^2$$
 (25)

s.t.
$$b_i^{\top} w \ge a_i, \quad i = 1, ..., m$$
 (26)

where

$$\nu_{\text{nom}} = M^{-1}(q) \left(\tau_{\text{nom}} - C(q, \dot{q}) \dot{q}(t) - G(q) - F(\dot{q}) \right) \quad (27)$$

and τ_{nom} is the nominal control torque. The filtered control torque can then be determined as

$$\tau_{\text{safe}} = M(q)\nu_{\text{safe}} + C(q, \dot{q})\dot{q}(t) + G(q) + F(\dot{q}). \quad (28)$$

We can now state our main result.

Theorem 1: If $q(0) \in \mathcal{H}$, and the controller parameter c is chosen such that (13) is satisfied, then the filtered controller (23)–(28) applied to the system (1) ensures that $q(t) \in \mathcal{H}$, $\forall t \in [0, T)$. Furthermore, the filtered torque τ_{safe} is uniformly bounded provided that the nominal torque τ_{nom} is continuous in t and Lipschitz in Q.

IV. PROOF OF THEOREM 1

To prove the invariance of the set \mathcal{H} during the interval $t \in [0, T)$, it is first necessary to show that the linear inequalities (26) always have a jointly feasible solution. To this end, we construct the following feasible solution:

$$\nu_{\text{feasible}} = -2c\mu_2 \dot{q} - J^+(q)\dot{J}(q)\dot{q}$$
 (29)

where $J^+(q)$ is the Moore–Penrose pseudoinverse of J(q). Note that due to Assumption 1, J(q) is nonsingular, and thus $J(q)J^+(q) = I$. Substituting (29) into the condition (26) yields

$$0 \ge -\dot{q}^{\top} J^{\top}(q) \frac{\partial^2 h_i}{\partial p^2} J(q) \dot{q} - c\mu_3 \left(\frac{2}{T} + c\mu_1\right) h_i. \tag{30}$$

Using the property (6), we can further simplify this inequality

$$0 \ge -c\mu_3 \left(\frac{2}{T} + c\mu_1\right) h_i \tag{31}$$

and thus we determine that for $q(t) \in \mathcal{H}$, (26) has a jointly feasible solution.

Next, we show that $q(0) \in \mathcal{H}$ ensures that $q(t) \in \mathcal{H}$, $\forall t \in [0, T)$. Through the application of the comparison Lemma to (15), we obtain the following inequality:

$$y_{i2}(t) \ge y_{i2}(0)e^{cT(1-\mu_1(t))} > 0 \quad \forall t \in [0, T).$$
 (32)

Integrating (14) from 0 to t, and substituting this inequality yields

$$y_{i1}(t) = y_{i1}(0)e^{cT(1-\mu_1(t))} + \int_0^t e^{cT(\mu_1(s)-\mu_1(t))}y_{i2}(s)ds$$

> $y_{i1}(0)e^{cT(1-\mu_1(t))} > 0 \quad \forall t \in [0, T).$ (33)

Through applying the relationship (11), we obtain

$$h_i(t) > 0 \quad \forall t \in [0, T) \tag{34}$$

and thus $q(t) \in \mathcal{H}, \forall t \in [0, T)$.

We now pursue the uniform boundedness of the filtered control law (23)–(28). We partition the time horizon [0, T) into separate intervals based on which CBFs h_i are active at time t. To this end, we define at time t the set of active constraints $\mathcal{A}(t)$ as

$$\mathcal{A}(t) = \left\{ i \in 1, \dots, m \middle| b_i^\top(t) v_{\text{safe}}(t) = a_i(t) \right\}$$
 (35)

where $a_i(t)$ and $b_i^{\top}(t)$ are defined in (23) and (24), respectively. Then, we define the partition times t_k

for $k \in \mathbb{N}$ with $t_0 = 0$ where

$$[0,T) = \bigcup_{\substack{k \in \mathbb{N} \cup \{0\} \\ t_{k+1} \le T}} [t_k, t_{k+1}). \tag{37}$$

We have constructed this partition such that the filtered control law (23)–(28) remains continuous at t_k .

We now examine the behavior of v_{safe} in the partition $[t_k, t_{k+1})$. If we have the condition $\mathcal{A}(t_k) = \emptyset$, then no constraints are active during this interval, and thus we have $v_{\text{safe}}(t) = v_{\text{nom}}(t)$ which is uniformly bounded.

If we have the condition $\mathcal{A}(t_k) \neq \emptyset$, then at least one constraint is active during the interval $[t_k, t_{k+1})$ and we do not necessarily have $\nu_{\text{safe}} = \nu_{\text{nom}}$. To determine a bound for ν_{safe} in this case, we first investigate the boundedness of the active CBFs h_i where $i \in \mathcal{A}(t_k)$. For each active barrier function, the output functions $y_{i1}(t)$ and $y_{i2}(t)$ satisfy the following differential equations:

$$\dot{y}_{i1}(t) = -c\mu_2(t)y_{i1}(t) + y_{i2}(t) \tag{38}$$

$$\dot{y}_{i2}(t) = -c\mu_2(t)y_{i2}(t). \tag{39}$$

Integrating these equations from t_k to t_{k+1} yields

$$y_{i1}(t) = (y_{i2}(t_k) + ty_{i2}(t_k))e^{cT(\mu_1(t_k) - \mu_1(t))}$$
(40)

$$y_{i2}(t) = y_{i2}(t_k)e^{cT(\mu_1(t_k) - \mu_1(t))}.$$
 (41)

Then, (40) can be substituted into (11) to obtain an expression for $h_i(t)$ and can be differentiated with respect to t to obtain an expression for $\dot{h}_i(t)$

$$h_i(t) = (y_{i2}(t_k) + ty_{i2}(t_k))e^{cT(\mu_1(t_k) - \mu_1(t))}$$
(42)

$$\dot{h}_{i}(t) = -c\mu_{2}(t)(y_{i2}(t_{k}) + ty_{i2}(t_{k}))e^{cT(\mu_{1}(t_{k}) - \mu_{1}(t))} + y_{i2}(t_{k})e^{cT(\mu_{1}(t_{k}) - \mu_{1}(t))}.$$
(43)

Due to the negative dominating behavior of the exponentials in (42) and (43), it can be seen that $h_i(t)$ and $\dot{h}_i(t)$ remain bounded within the interval $[t_k, t_{k+1})$. Furthermore, if $t_{k+1} = T$, we can use l'Hôpital's rule to determine the behavior of the active CBFs as the terminal time is approached

$$\lim_{t \to T^{-}} h_{i}(t) = \lim_{t \to T^{-}} \dot{h}_{i}(t) = 0 \quad \forall i \in \mathcal{A}(t_{k}).$$
 (44)

Thus, the active CBFs remain bounded in the interval $[t_k, t_{k+1})$ and approach 0 if $t_{k+1} = T$.

Using the boundedness of $\dot{h}_i(t)$, we now investigate the boundedness of q and \dot{q} within the interval $[t_k, t_{k+1})$. Differentiating the expression $h_i(p(q(t)))$ yields

$$\dot{h}_i = \frac{\partial q}{\partial p} J(q) \dot{q} = b_i^{\top} \dot{q}$$
 (45)

where b_i^{\top} is initially defined in (24). Thus, the component of \dot{q} that is parallel to b_i^{\top} is bounded and approaches 0 if $t_{k+1} = T$. As this property holds for each b_i^{\top} where $i \in \mathcal{A}(t_k)$, we deduce the following properties of \dot{q} :

$$\left|B\dot{q}\right| < \infty \quad \forall t \in \left[t_k, t_{k+1}\right)$$
 (46)

$$\lim_{t \to T^{-}} B\dot{q} = 0, \quad \text{if} \quad t_{k+1} = T \tag{47}$$

where B is a projection matrix to the minimum subspace spanned by the vectors b_i^{T} where $i \in \mathcal{A}(t_k)$. Using this

projection matrix, we separate \dot{q} into the components that lie within and outside of this minimum subspace

$$\dot{q} = \dot{q}_{\parallel} + \dot{q}_{\perp} \tag{48}$$

where

$$\dot{q}_{\parallel} = B\dot{q} \tag{49}$$

$$\dot{q}_{\perp} = (I - B)\dot{q}. \tag{50}$$

From integrating \dot{q}_{\parallel} , we can additionally obtain the boundedness of $q_{\parallel}=Bq$.

Next, we obtain the boundedness of q_{\perp} and \dot{q}_{\perp} . We make use of the fact that since $\nu_{\rm safe}$ is obtained via quadratic programming, the difference between the safe and nominal control $\nu_{\rm safe} - \nu_{\rm nom}$ lies in the subspace spanned by B, and thus we have $\nu_{\rm safe, \perp} = \nu_{\rm nom, \perp}$. This property can be verified by contradiction, as for every feasible solution where this property does not hold, a feasible solution with a lower value of the objective function $\|w - \nu_{\rm nom}\|^2$ can be obtained via eliminating the perpendicular component of $w - \nu_{\rm nom}$. Thus, q_{\perp} and \dot{q}_{\perp} satisfy the following differential equations:

$$\dot{q}_{\perp} = q_{\perp} \tag{51}$$

$$\ddot{q}_{\perp} = \nu_{\text{nom},\perp}.\tag{52}$$

As ν_{nom} is continuous in t and Lipschitz in Q, and q_{\parallel} and \dot{q}_{\parallel} are bounded, these differential equations can be integrated from t_k to t_{k+1} to simultaneously obtain the boundedness of ν_{nom} , q_{\perp} and \dot{q}_{\perp} , and consequently q and \dot{q} .

To determine a bound for v_{safe} , we first investigate the boundedness of the following feasible solution:

$$v_{\text{alt}} = -2c\mu_2 \dot{q}_{\parallel} - J^{+}(q)\dot{J}(q)\dot{q}$$
 (53)

in which we have replaced \dot{q} in the first term of (29) with \dot{q}_{\parallel} , noting that this does not alter the feasibility of the solution. Through the application of Assumption 1, it can be observed that the second term in (53) is bounded in the interval $[t_k, t_{k+1})$. To bound the first term in (53), we use l'Hôpital's rule to obtain the following limit:

$$\lim_{t \to T^{-}} \mu_{2}(t)\dot{h}_{i}(t) = 0 \quad \forall i \in \mathcal{A}(t_{k}).$$
 (54)

Applying this limit and (45) to the first term in (53), it can be observed that this term and consequently v_{alt} are bounded within the interval $[t_k, t_{k+1})$. Then, it can be seen from (25) that we must also have

$$v_{\text{safe}} \le \|v_{\text{alt}} - v_{\text{nom}}\|^2 \tag{55}$$

and thus $\nu_{\rm safe}$ is bounded in the interval $[t_k, t_{k+1})$. As we have determined that $\nu_{\rm safe}$ is bounded in each interval $[t_k, t_{k+1})$, we conclude that $\nu_{\rm safe}$ and consequently $\tau_{\rm safe}$ are uniformly bound in the interval [0, T).

V. SIMULATED AND EXPERIMENTAL RESULTS

To assess the performance of the proposed PTSf approach, we perform both the simulations using the ODE methods on Baxter's dynamic equation (1), as well as experiments. In both the simulation and experiment, Baxter must track a 6-s trajectory designed for a pick-and-place task in [13],

while simultaneously avoiding collision with a large spherical obstacle blocking the trajectory and placing its held object precisely on the surface of a table. It is important to note that this trajectory was designed such that the maximum required torque to follow the trajectory when there are no obstacles to avoid is much less than Baxter's maximum torque output. Due to this conservative specification, Baxter's maximum torque output does not affect the results of our simulations and experiments. To highlight the ability of this method to allow convergence to the barrier within a finite period of time, the nominal controller used in both the simulations and experiments is a prescribed-time controller which we previously formulated in [18]. As we demonstrated in this earlier work, this prescribed-time nominal controller is capable of achieving zero tracking errors by the end of the 6-s desired trajectory. Thus, our simulations and experiments will serve to demonstrate the ability of the proposed PTSf method to allow convergence to the barrier within a finite period of time. Furthermore, we compare the performance of the PTSf method presented here to an ESf with a high gain, as well as an ESf with a low gain to highlight the strengths of the proposed method.

In the simulations and experiments, the CBF preventing collision with the spherical obstacle is formulated as

$$h_1(p(q)) = \|p(q) - p_{\text{sphere}}\|_2^2 - R_{\text{sphere}}^2$$
 (56)

where $p_{\text{sphere}} \in \mathbb{R}^3$ is the position of the sphere, and $R_{\text{sphere}} \in \mathbb{R}$ is the minimum safe distance between the robot manipulator and the center of the obstacle. We formulate the CBF preventing collision with the table as

$$h_2(p(q)) = p(q) \cdot (0, 0, 1) - z_{\text{table}}$$
 (57)

where $z_{\text{table}} \in \mathbb{R}$ is the height of the table. For the PTSf, we set the controller parameter as c=1.2. To prevent numerical issues arising from using an unbounded scaling of the gain μ_2 , we clip this scaling at a maximum value $\mu_{2,\text{max}} = 6.25$. A consequence of this modification is that the robot manipulator is allowed to reach a small neighborhood of the barrier as the terminal time is approached, rather than reaching the barrier exactly as when using an unbounded gain. For our 6-s task, this maximum is reached after 3.6 s of operation and was chosen so that the previously mentioned neighborhood is negligible, and thus performance is qualitatively similar to that of using an unbounded gain. For the nominal controller, we use the same controller parameters as in [18], so that the interested reader can compare the performance of the PTSf + nominal controller to that of the nominal controller alone.

To convert our formulation of a PTSf into that of an ESf, the following expression can be used in substitute of (23):

$$a_{i,\text{esf}} = -\dot{q}^{\top} J^{\top}(q) \frac{\partial^{2} h_{i}}{\partial p^{2}} J(q) \dot{q} - \frac{\partial h_{i}}{\partial p} \dot{J}(q) \dot{q}$$
$$-2\rho^{2} h_{i} - 3\rho \frac{\partial h_{i}}{\partial p} J(q) \dot{q} \qquad (58)$$

with $\rho > 0$. For our high gain ESf, we set $\rho = 4$ so that the high gain ESf + nominal controller can achieve negligible tracking error at the end of the 6-s task. For our low gain ESf,

we instead set $\rho = 1.5$ so that the low-gain ESf begins to take evasive action at the same instance of time as the proposed PTSf.

From Fig. 3, it can be observed that the proposed PTSf successfully avoids the spherical obstacle in both the simulation and experiment, while simultaneously placing the held object precisely on the table at the end of the 6-s task. Check the DSCL YouTube Channel, at https://youtu.be/yRr6D2oFSeQ, for the video of Baxter performing the experiment. Furthermore, the magnitude of the torque applied by the PTSf gradually increases as the spherical obstacle is approached, indicating that the control action is smooth and that the magnitude of the joint jerks of Baxter is not large. In comparison, the ESf with a high gain is also successful at placing the held object precisely on the table. However, the magnitude of the torque applied by the PTSf increases much more rapidly as the obstacle is approached, indicating a sharper discontinuity in the control action and higher joint jerks. Conversely, the ESf with a low gain appears to have joint jerks with a similar magnitude as that of the proposed PTSf, but is unable to achieve zero tracking error by the end of the 6-s task. Unlike both the PTSf and the ESf with a high gain, the ESf with a low gain becomes active toward the end of the task, limiting the rate of approach to the table to a slow exponential approach, rather than the prescribed-time approach governed by the nominal controller. The ability of the PTSf to behave in a desirable manner in both avoiding the spherical obstacle without high joint jerks and placing the held object precisely on the table at the end of the 6-s task can be traced back to the design of the output function $y_{i2}(t)$ in (12). As both $y_{i1}(t)$ and $y_{i2}(t)$ must remain positive to ensure safety, the scaling function $\mu_2(t)$ allows the robot manipulator to approach obstacles more quickly as the terminal time is approached, thus causing the PTSf to become less conservative. Thus, the PTSf behaves similar to the low gain ESf in the beginning of the procedure, and similar to the high gain ESF in the end of the procedure. The distance between the end-effector and the nearest obstacle in both the simulation and experiment can be more closely observed in Fig. 4. While the PTSf and high gain ESf are able to place the held object precisely on the table, the lowgain ESf instead holds the object roughly 1 cm above the table by the end of the 6-s task. In addition, it is notable to mention that the ESf with a low gain appears to behave much more conservatively in the experiment than in the simulation, maintaining a large distance between the end-effector and the spherical obstacle. This is likely due to a discrepancy between the modeled and actual friction in each joint of Baxter and is more apparent when the filter gains are not large enough to counteract their contribution.

In Fig. 5, the magnitude of the difference between the nominal and filtered joint torques, $\|\tau_{\text{safe}} - \tau_{\text{nom}}\|_2$, can be seen. It can be observed from this figure that the PTSf and the low-gain ESf become active after around 1 s of operation, whereas the high-gain ESf becomes active after around 2 s of operation. To avoid collision with the spherical obstacle while reacting at a later time, the high-gain ESf ramps up in magnitude much faster than the PTSf and low-gain ESf, indicating larger joint jerks during the operation of the robot manipulator at this time.

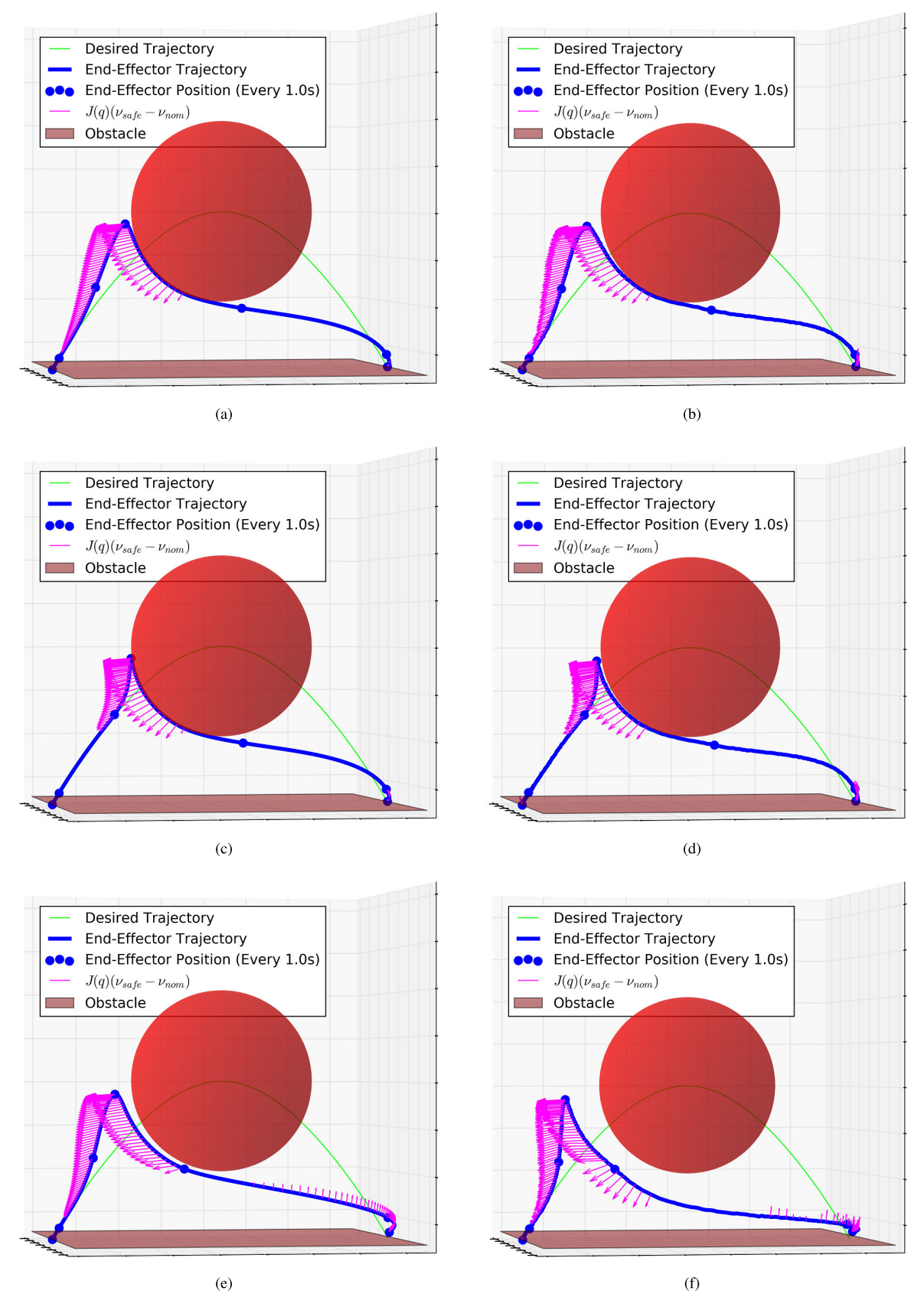


Fig. 3. Simulations (left column) and experiments (right column) of Baxter following a pick-and-place trajectory while avoiding multiple obstacles, using (a) and (b) PTSf, (c) and (d) ESf with a high gain of $\rho = 4$, and (e) and (f) ESf with a low gain of $\rho = 1.5$. At t = 3 s, the end-effector trajectory takes a major turn from moving up to moving below the spherical obstacle.

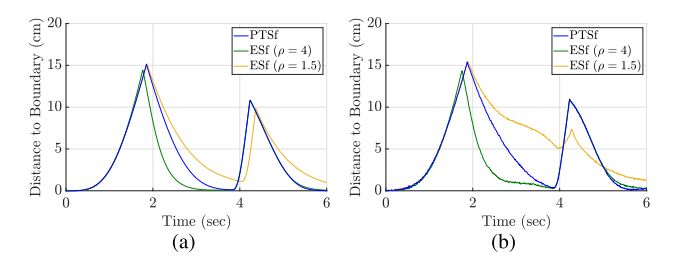


Fig. 4. (a) Simulated and (b) experimental distance between the robot manipulator and the nearest obstacle.

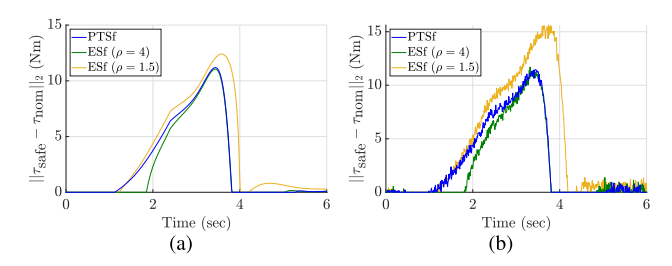


Fig. 5. Magnitude of the difference between the nominal and filtered joint torques in (a) simulation and (b) experiment.

After around 4 s of operation, each safety filter rapidly drops in magnitude. This period in time corresponds to the endeffector quickly passing under the spherical obstacle, meaning that the obstacle is no longer blocking the end-effector from approaching the reference trajectory. Thus, this large change in magnitude of each safety filter is primarily due to the shape of the obstacle CBF, as well as the nominal controller rather than the convergence properties of the used safety filter. It is important to mention that at this instant, the safety filter with the highest experienced joint jerks is the low-gain ESf. This is due to the conservative low gains of the ESf keeping the endeffector further from the reference trajectory in the beginning of the task, resulting in a larger nominal control torque to drive the system back toward the reference trajectory. During the last 2 s of the task, the low-gain ESf maintains operation with a small magnitude, while both the high gain ESf and the PTSf do not noticably interfere with the motion of the end-effector at this time.

The experimental, simulated, and desired joint trajectories of Baxter can be seen in Fig. 6. To avoid the large spherical obstacle, joints 1 and 3 experience large deviations from the desired trajectory, with the low-gain ESf experiencing the largest tracking errors. After this large deviation, the joint trajectories smoothly converge back to the desired trajectory. Observing Fig. 7, it is possible to see the convergence behavior of each method in more detail. While the tracking errors for the PTSf and high-gain ESf reach negligible values, there is a residual tracking error of roughly one degree on joint 2 for the low-gain ESf. This joint is primarily responsible for the height of the end-effector, and thus this tracking error is present due to the low-gain ESf limiting the rate of approach to the table.

The experimental and simulated joint toque input signals of Baxter can be seen in Fig. 8. It is important to note that these torques are significantly lower than the maximum torque output of Baxter's joints, which are $50 \text{ N} \cdot \text{m}$ for joints 1-4, and $15 \text{ N} \cdot \text{m}$ for joints 5-7. Thus, none of the tested methods

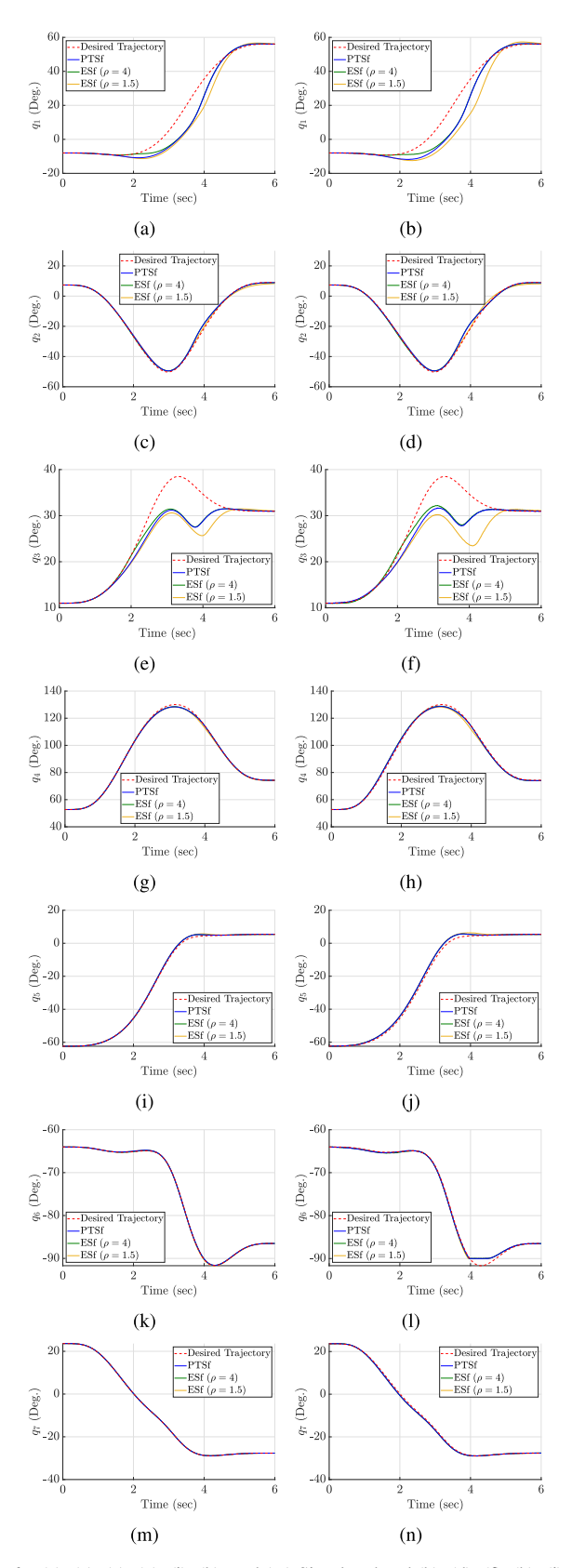


Fig. 6. (a), (c), (e), (g), (i), (k), and (m) Simulated and (b), (d), (f), (h), (j), (l), and (n) experimental joint trajectories of Baxter. At t=3 s, the end-effector trajectory takes a major turn from moving up to moving below the spherical obstacle.

poses the risk of torque saturation. Furthermore, while the presence of noise in angular velocity measurements has caused

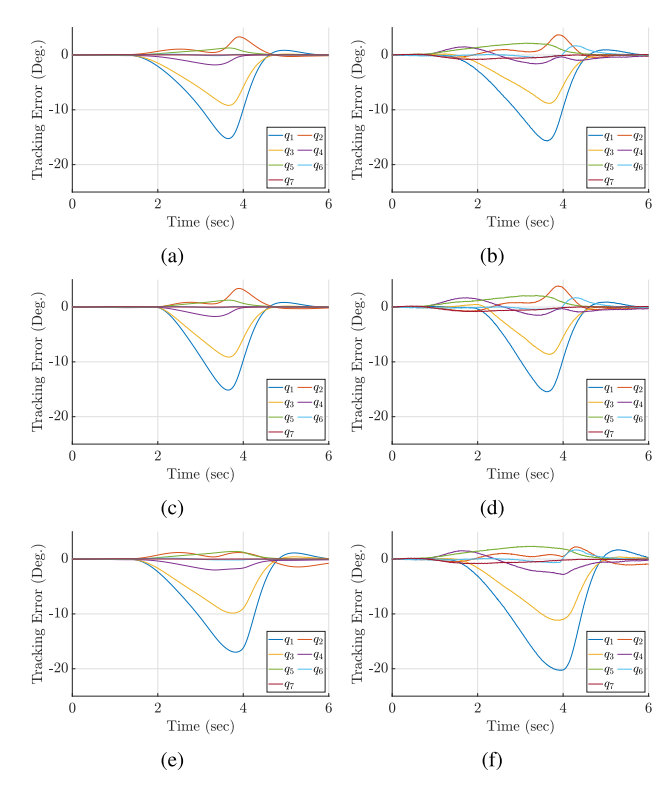


Fig. 7. Simulated (left column) and experimental (right column) tracking errors of Baxter when using (a) and (b) PTSf, (c) and (d) ESf with a high gain of $\rho=4$, and (e) and (f) ESf with a low gain of $\rho=1.5$.

similar variations in the experimental joint torques, these torques still exhibit moderate continuity and do not appear to be affected by chattering. There does not appear to be a large difference between the tested methods with regards to their susceptibility to noise, as each curve appears to have a similar degree of "fuzziness."

The simulated joint jerks of Baxter when the safety filter is active can be seen in Fig. 9. In the beginning of the task, the joint jerk from the high-gain ESf is an order of magnitude larger than either the PTSf or the low-gain ESf. As the task progresses, the jerk from the high-gain ESf becomes nearly identical to that of the PTSf, due to the end-effector following along the surface of the spherical obstacle. At the end of the task, both the PTSf and the high-gain ESf have a negligible joint jerk compared with the low-gain ESf, which actively limits the rate of approach of the end-effector to the surface of the table. Across the duration of the task, the PTSf consistently achieves the smallest joint jerks out of the tested methods, only increasing in magnitude due to the influence of the shape of the obstacle and the trajectory tracking task.

It is important to note that the path of the end-effector when using a PTSf, as with CBF approaches in general, depends on the structure of the barrier functions h_i . For example in Fig. 10(a), lowering the center of the spherical obstacle by 120 mm causes the end-effector trajectory to go over the spherical obstacle rather than below it. Furthermore, as the quadratic programming filter strategy (25), (26) is a local optimization scheme, it is possible for the end-effector to get stuck on an obstacle even when there is a valid path back to the reference trajectory. In Fig. 10(b), by lowering the spherical

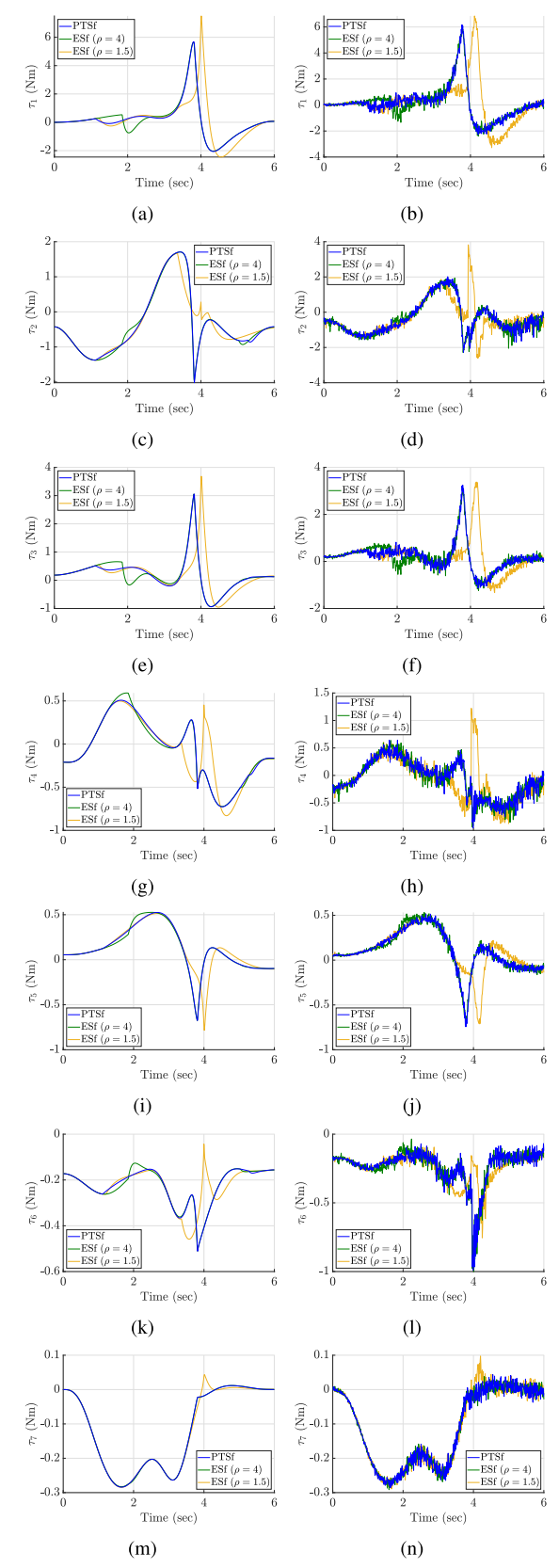


Fig. 8. (a), (c), (e), (g), (i), (k), and (m) Simulated and (b), (d), (f), (h), (j), (l), and (n) experimental joint torque input signals of Baxter. At t=3 s, the end-effector trajectory takes a major turn from moving up to moving below the spherical obstacle.

obstacle precisely 67 mm, the end-effector is no longer able to return to the reference trajectory. Even in this case however,

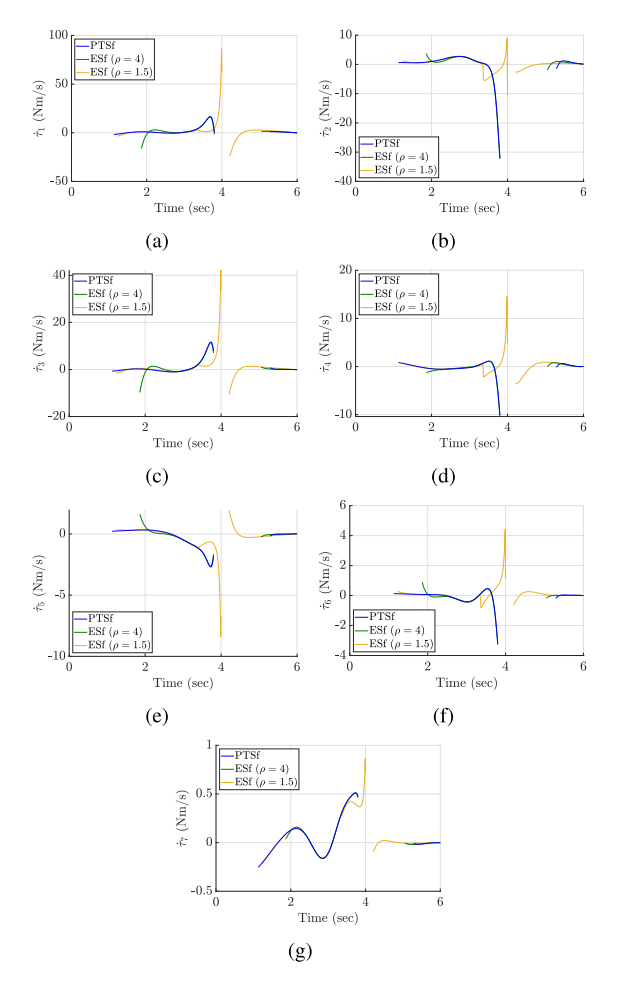


Fig. 9. (a)–(g) Simulated joint jerks of Baxter, shown when the safety filter is active. At t = 3 s, the end-effector trajectory takes a major turn from moving up to moving below the spherical obstacle.

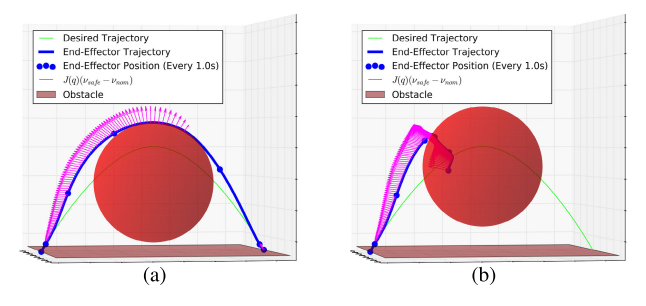


Fig. 10. Simulations of Baxter following a pick-and-place trajectory while avoiding multiple obstacles, using a PTSf. In (a), the center of the spherical obstacle is lowered 120 mm, resulting in the end-effector going over the spherical obstacle. In (b), the center of the spherical obstacle is lowered exactly 67 mm, resulting in the end-effector being unable to reach its destination. Note that in this case, the end-effector still travels along the surface of the spherical obstacle without exiting the safe set.

the end-effector does not violate the safe set, and instead gently comes into contact with the spherical obstacle at the end of the 6-s task. The primary purpose of our proposed PTSf and ESfs and other CBF-based approaches is to ensure the system does not leave the safe set in a minimally invasive manner. In the context of safety, these approaches should not be seen as a substitute for path-planning, but instead as an additional layer of safety, ensuring the system remains safe even when

the system does not perfectly follow the reference trajectory, or if the reference trajectory is not suitably designed to prevent collision with obstacles.

VI. CONCLUSION

In this research effort, we reformulated the PTSf initially proposed by Abel et al. [1] for the case of a redundant manipulator performing a fixed-duration task. This formulation yields a filter that is capable of avoiding multiple obstacles in a minimally invasive manner with bounded joint torques, while simultaneously allowing the nominal controller to converge to positions located on the boundary of the safe set by the end of the fixed-duration task. To demonstrate the efficacy of the proposed method, we performed a series of simulations and experiments on Baxter, a seven-DOF collaborative robot manipulator. In these simulations and experiments, Baxter must follow a 6-s parabolic trajectory as closely as possible while navigating around a large spherical obstacle blocking its path and place an object precisely on the surface of a table without overshoot by the end of the 6 s. To highlight the ability of this method to allow convergence to the barrier within a finite period of time, the nominal controller used in both the simulation and experiment is a prescribed-time controller which we previously formulated in [18]. The results of our simulations and experiments demonstrated the ability of the PTSf to enforce safety throughout the 6-s task, while allowing the robot manipulator to make contact with the table and thus achieve the desired goal position by the end of the task. Furthermore, when compared with the ESf, which is the state-of-the-art in current literature, our proposed method yielded consistently lower joint jerks. Thus, for tasks with a fixed duration, the proposed PTSf offers performance benefits over the exponential filters currently present in literature.

ACKNOWLEDGMENT

The views and opinions of authors expressed herein do not necessarily state or reflect those of the United States Government or any agency thereof.

REFERENCES

- [1] I. Abel, D. Steeves, M. Krstic, and M. Jankovic, "Prescribed-time safety design for a chain of integrators," 2022, arXiv:2201.09447.
- [2] A. D. Ames, S. Coogan, M. Egerstedt, G. Notomista, K. Sreenath, and P. Tabuada, "Control barrier functions: Theory and applications," in *Proc.* 18th Eur. Control Conf. (ECC), Jun. 2019, pp. 3420–3431.
- [3] M. Bagheri, M. Krstić, and P. Naseradinmousavi, "Analytical and experimental predictor-based time delay control of Baxter robot," in *Proc. ASME Dyn. Syst. Control Conf.*, vol. 1, Oct. 2018, Art. no. V001T04A011.
- [4] M. Bagheri, M. Krstic, and P. Naseradinmousavi, "Joint-space trajectory optimization of a 7-DOF Baxter using multivariable extremum seeking," in *Proc. Annu. Amer. Control Conf. (ACC)*, Milwaukee, WI, USA, Jun. 2018, pp. 2176–2181.
- [5] M. Bagheri, M. Krstić, and P. Naseradinmousavi, "Multivariable extremum seeking for joint-space trajectory optimization of a highdegrees-of-freedom robot," J. Dyn. Syst., Meas., Control, vol. 140, no. 11, Nov. 2018, Art. no. 111017.
- [6] M. Bagheri and P. Naseradinmousavi, "Novel analytical and experimental trajectory optimization of a 7-DOF Baxter robot: Global design sensitivity and step size analyses," *Int. J. Adv. Manuf. Technol.*, vol. 93, nos. 9–12, pp. 4153–4167, Dec. 2017.

- [7] M. Bagheri, P. Naseradinmousavi, and M. Krstić, "Feedback linearization based predictor for time delay control of a high-DOF robot manipulator," *Automatica*, vol. 108, Oct. 2019, Art. no. 108485.
- [8] M. Bagheri, P. Naseradinmousavi, and M. Krstić, "Time delay control of a high-DOF robot manipulator through feedback linearization based predictor," in *Proc. Dyn. Syst. Control Conf.*, vol. 59162, 2019, Art. no. V003T16A001.
- [9] M. Bagheri, P. Naseradinmousavi, and R. Morsi, "Experimental and novel analytical trajectory optimization of a 7-DOF Baxter robot: Global design sensitivity and step size analyses," in *Proc. ASME Dyn. Syst. Control Conf.*, vol. 1, Oct. 2017, Art. no. V001T30A001.
- [10] E. A. Basso and K. Y. Pettersen, "Task-priority control of redundant robotic systems using control Lyapunov and control barrier function based quadratic programs," *IFAC-PapersOnLine*, vol. 53, no. 2, pp. 9037–9044, 2020.
- [11] A. Bauer, D. Wollherr, and M. Buss, "Human-robot collaboration: A survey," *Int. J. Humanoid Robot.*, vol. 5, no. 1, pp. 47–66, Mar. 2008.
- [12] H. M. Becerra, C. R. Vazquez, G. Arechavaleta, and J. Delfin, "Predefined-time convergence control for high-order integrator systems using time base generators," *IEEE Trans. Control Syst. Technol.*, vol. 26, no. 5, pp. 1866–1873, Sep. 2018.
- [13] A. Bertino, M. Bagheri, M. Krstić, and P. Naseradinmousavi, "Experimental autonomous deep learning-based 3D path planning for a 7-DOF robot manipulator," in *Proc. Dyn. Syst. Control Conf.*, vol. 2, Oct. 2019, Art. no. V002T14A002.
- [14] A. Bertino, P. Naseradinmousavi, and A. Kelkar, "Experimental and analytical decentralized adaptive control of a 7-DOF robot manipulator," in *Proc. Dyn. Syst. Control Conf.*, vol. 84270, 2020, Art. no. V001T05A004.
- [15] A. Bertino, P. Naseradinmousavi, and A. Kelkar, "Analytical and experimental decentralized adaptive control of a high-degrees-of-freedom robot manipulator," *J. Dyn. Syst., Meas., Control*, vol. 143, no. 7, Jul. 2021, Art. no. 071007.
- [16] A. Bertino, P. Naseradinmousavi, and M. Krstic, "Experimental and analytical delay-adaptive control of a 7-DOF robot manipulator," in *Proc. Amer. Control Conf. (ACC)*, May 2021, pp. 72–77.
- [17] A. Bertino, P. Naseradinmousavi, and M. Krstic, "Delay-adaptive control of a 7-DOF robot manipulator: Design and experiments," *IEEE Trans. Control Syst. Technol.*, vol. 30, no. 6, pp. 2506–2521, Nov. 2022.
- [18] A. Bertino, P. Naseradinmousavi, and M. Krstic, "Experimental and analytical prescribed-time trajectory tracking control of a 7-DOF robot manipulator," in *Proc. Amer. Control Conf. (ACC)*, Jun. 2022, pp. 1941–1946.
- [19] A. Billard and D. Kragic, "Trends and challenges in robot manipulation," *Science*, vol. 364, no. 6446, Jun. 2019, Art. no. eaat8414.
- [20] Y. Cao, J. Cao, and Y. Song, "Practical prescribed time control of Euler-Lagrange systems with partial/full state constraints: A settling time regulator-based approach," *IEEE Trans. Cybern.*, vol. 52, no. 12, pp. 13096–13105, Dec. 2022.
- [21] Y. Cao and Y.-D. Song, "Adaptive PID-like fault-tolerant control for robot manipulators with given performance specifications," *Int. J. Control*, vol. 93, no. 3, pp. 377–386, Mar. 2020.
- [22] Y. Chen, A. Singletary, and A. D. Ames, "Guaranteed obstacle avoidance for multi-robot operations with limited actuation: A control barrier function approach," *IEEE Control Syst. Lett.*, vol. 5, no. 1, pp. 127–132, Jan. 2021.
- [23] R. Cheng, M. J. Khojasteh, A. D. Ames, and J. W. Burdick, "Safe multi-agent interaction through robust control barrier functions with learned uncertainties," in *Proc. 59th IEEE Conf. Decis. Control (CDC)*, Dec. 2020, pp. 777–783.
- [24] C.-S. Chung, H. Wang, and R. A. Cooper, "Functional assessment and performance evaluation for assistive robotic manipulators: Literature review," *J. Spinal Cord Med.*, vol. 36, no. 4, pp. 273–289, 2013.
- [25] W. S. Cortez and D. V. Dimarogonas, "Correct-by-design control barrier functions for Euler–Lagrange systems with input constraints," in *Proc. Amer. Control Conf. (ACC)*, Jul. 2020, pp. 950–955.
- [26] A. De Santis, B. Siciliano, A. De Luca, and A. Bicchi, "An atlas of physical human–robot interaction," *Mech. Mach. Theory*, vol. 43, no. 3, pp. 253–270. Mar. 2008.
- [27] N. Espitia, A. Polyakov, D. Efimov, and W. Perruquetti, "Boundary time-varying feedbacks for fixed-time stabilization of constant-parameter reaction-diffusion systems," *Automatica*, vol. 103, pp. 398–407, May 2019.

- [28] A. W. Farras and T. Hatanaka, "Safe control with control barrier function for Euler-Lagrange systems facing position constraint," in *Proc. SICE Int. Symp. Control Syst.*, Mar. 2021, pp. 28–32.
- [29] R. T. Fawcett, A. Pandala, A. D. Ames, and K. A. Hamed, "Robust stabilization of periodic gaits for quadrupedal locomotion via QPbased virtual constraint controllers," *IEEE Control Syst. Lett.*, vol. 6, pp. 1736–1741, 2022.
- [30] F. Ferraguti, M. Bertuletti, C. T. Landi, M. Bonfe, C. Fantuzzi, and C. Secchi, "A control barrier function approach for maximizing performance while fulfilling to ISO/TS 15066 regulations," *IEEE Robot. Autom. Lett.*, vol. 5, no. 4, pp. 5921–5928, Oct. 2020.
- [31] K. Garg and D. Panagou, "Robust control barrier and control Lyapunov functions with fixed-time convergence guarantees," in *Proc. Amer. Con*trol Conf. (ACC), May 2021, pp. 2292–2297.
- [32] S. I. Han and J. Lee, "Finite-time sliding surface constrained control for a robot manipulator with an unknown deadzone and disturbance," ISA Trans., vol. 65, pp. 307–318, Nov. 2016.
- [33] J. Holloway and M. Krstic, "Prescribed-time observers for linear systems in observer canonical form," *IEEE Trans. Autom. Control*, vol. 64, no. 9, pp. 3905–3912, Sep. 2019.
- [34] Y. Hong, Y. Xu, and J. Huang, "Finite-time control for robot manipulators," Syst. Control Lett., vol. 46, no. 4, pp. 243–253, Jul. 2002.
- [35] S.-C. Hsu, X. Xu, and A. D. Ames, "Control barrier function based quadratic programs with application to bipedal robotic walking," in *Proc. Amer. Control Conf. (ACC)*, Jul. 2015, pp. 4542–4548.
- [36] X. Jin, "Adaptive fixed-time control for MIMO nonlinear systems with asymmetric output constraints using universal barrier functions," *IEEE Trans. Autom. Control*, vol. 64, no. 7, pp. 3046–3053, Jul. 2019.
- [37] V. R. Kamidi, J. Kim, R. T. Fawcett, A. D. Ames, and K. A. Hamed, "Distributed quadratic programming-based nonlinear controllers for periodic gaits on legged robots," *IEEE Control Syst. Lett.*, vol. 6, pp. 2509–2514, 2022.
- [38] P. Krishnamurthy, F. Khorrami, and M. Krstic, "A dynamic high-gain design for prescribed-time regulation of nonlinear systems," *Automatica*, vol. 115, May 2020, Art. no. 108860.
- [39] P. Krishnamurthy, F. Khorrami, and M. Krstic, "Adaptive output-feedback stabilization in prescribed time for nonlinear systems with unknown parameters coupled with unmeasured states," *Int. J. Adapt. Control Signal Process.*, vol. 35, no. 2, pp. 184–202, Feb. 2021.
- [40] V. Kurtz, P. M. Wensing, and H. Lin, "Control barrier functions for singularity avoidance in passivity-based manipulator control," 2021, arXiv:2109.13349.
- [41] C. T. Landi, F. Ferraguti, S. Costi, M. Bonfe, and C. Secchi, "Safety barrier functions for human–robot interaction with industrial manipulators," in *Proc. 18th Eur. Control Conf. (ECC)*, Jun. 2019, pp. 2565–2570.
- [42] W. Li and M. Krstic, "Stochastic nonlinear prescribed-time stabilization and inverse optimality," *IEEE Trans. Autom. Control*, vol. 67, no. 3, pp. 1179–1193, Mar. 2021.
- [43] M. Lippi and A. Marino, "A control barrier function approach to human-multi-robot safe interaction," in *Proc. 29th Medit. Conf. Control Autom.* (MED), Jun. 2021, pp. 604–609.
- [44] A. J. Muñoz-Vázquez, J. D. Sánchez-Torres, E. Jiménez-Rodríguez, and A. G. Loukianov, "Predefined-time robust stabilization of robotic manipulators," *IEEE/ASME Trans. Mechatronics*, vol. 24, no. 3, pp. 1033–1040, Jun. 2019.
- [45] Q. Nguyen and K. Sreenath, "Exponential control barrier functions for enforcing high relative-degree safety-critical constraints," in *Proc. Amer. Control Conf. (ACC)*, Jul. 2016, pp. 322–328.
- [46] J. Obregon-Flores, G. Arechavaleta, H. M. Becerra, and A. Morales-Diaz, "Predefined-time robust hierarchical inverse dynamics on torque-controlled redundant manipulators," *IEEE Trans. Robot.*, vol. 37, no. 3, pp. 962–978, Jun. 2021.
- [47] M. Rauscher, M. Kimmel, and S. Hirche, "Constrained robot control using control barrier functions," in *Proc. IEEE/RSJ Int. Conf. Intell. Robots Syst. (IROS)*, Oct. 2016, pp. 279–285.
- [48] S. Robla-Gómez, V. M. Becerra, J. R. Llata, E. González-Sarabia, C. Torre-Ferrero, and J. Pérez-Oria, "Working together: A review on safe human–robot collaboration in industrial environments," *IEEE Access*, vol. 5, pp. 26754–26773, 2017.
- [49] J. D. Sánchez-Torres, A. J. Muñoz-Vázquez, M. Defoort, E. Jiménez-Rodríguez, and A. G. Loukianov, "A class of predefined-time controllers for uncertain second-order systems," *Eur. J. Control*, vol. 53, pp. 52–58, May 2020.

- [50] A. Singletary, S. Kolathaya, and A. D. Ames, "Safety-critical kinematic control of robotic systems," *IEEE Control Syst. Lett.*, vol. 6, pp. 139–144, 2022.
- [51] Y. Song, Y. Wang, J. Holloway, and M. Krstic, "Time-varying feedback for regulation of normal-form nonlinear systems in prescribed finite time," *Automatica*, vol. 83, pp. 243–251, Sep. 2017.
- [52] Y. Song, Y. Wang, and M. Krstic, "Time-varying feedback for stabilization in prescribed finite time," *Int. J. Robust Nonlinear Control.*, vol. 29, no. 3, pp. 618–633, Mar. 2018.
- [53] D. Steeves, M. Krstic, and R. Vazquez, "Prescribed-time estimation and output regulation of the linearized Schrödinger equation by backstepping," *Eur. J. Control*, vol. 55, pp. 3–13, Jan. 2020.
- [54] Y. Su, C. Zheng, and P. Mercorelli, "Robust approximate fixed-time tracking control for uncertain robot manipulators," *Mech. Syst. Signal Process.*, vol. 135, Jan. 2020, Art. no. 106379.
- [55] H. Wang, J. Peng, F. Zhang, H. Zhang, and Y. Wang, "High-order control barrier functions-based impedance control of a robotic manipulator with time-varying output constraints," *ISA Trans.*, vol. 129, pp. 361–369, Oct. 2022.
- [56] Y. Wang, M. Chen, and Y. Song, "Robust fixed-time inverse dynamic control for uncertain robot manipulator system," *Complexity*, vol. 2021, pp. 1–12, Jan. 2021.
- [57] Y. Wang and X. Xu, "Disturbance observer-based robust control barrier functions," 2022, arXiv:2203.12855.
- [58] C. Yang, Y. Jiang, W. He, J. Na, Z. Li, and B. Xu, "Adaptive parameter estimation and control design for robot manipulators with finite-time convergence," *IEEE Trans. Ind. Electron.*, vol. 65, no. 10, pp. 8112–8123. Oct. 2018.
- [59] S. Yu, X. Yu, B. Shirinzadeh, and Z. Man, "Continuous finite-time control for robotic manipulators with terminal sliding mode," *Automatica*, vol. 41, no. 11, pp. 1957–1964, Nov. 2005.
- [60] D. Zhang, L. Kong, S. Zhang, Q. Li, and Q. Fu, "Neural networks-based fixed-time control for a robot with uncertainties and input deadzone," *Neurocomputing*, vol. 390, pp. 139–147, May 2020.
- [61] L. Zhang, Y. Wang, Y. Hou, and H. Li, "Fixed-time sliding mode control for uncertain robot manipulators," *IEEE Access*, vol. 7, pp. 149750–149763, 2019.
- [62] D. Zhao, F. Gao, S. Li, and Q. Zhu, "Robust finite-time control approach for robotic manipulators," *IET Control Theory Appl.*, vol. 4, no. 1, pp. 1–15, Jan. 2010.



Alexander Bertino received the B.Sc. degree in mechanical engineering from the University of California at San Diego, La Jolla, CA, USA, in 2017, and the M.Sc. degree in mechanical engineering from San Diego State University, San Diego, CA, USA, in 2019. He is currently pursuing the Ph.D. degree in mechanical engineering with San Diego State University and the University of California at San Diego.

He is currently working as a Research Assistant with the Dynamic Systems and Controls Laboratory,

San Diego State University. His research interests include robotics, control theory, adaptive control, delay systems, and machine learning.

Mr. Bertino has received the 2020 DSCD Robotics TC Best Student Paper for the research paper titled "Experimental and Analytical Decentralized Adaptive Control of a 7-DOF Robot Manipulator."



Peiman Naseradinmousavi received the B.Sc. degree in mechanical engineering (dynamics and control) from Tabriz University, Tabriz, Iran, in 2002, and the Ph.D. degree in mechanical engineering (dynamics and control) from Villanova University, Villanova, PA, USA, in 2012.

He is currently an Associate Professor with the Department of Mechanical Engineering, Dynamic Systems and Control Laboratory (DSCL), San Diego State University, San Diego, CA, USA. His research interests include robotics, smart flow distribution

networks, nonlinear dynamics, control theory, optimization, magnetic bearings, and mathematical modeling.

Dr. Naseradinmousavi was a recipient of the John J. Gallen Memorial Alumni Award in 2021. He serves as an Associate Editor for ASME Letters in Dynamic Systems and Control and the Journal of Vibration and Control (JVC).



Miroslav Krstić (Fellow, IEEE) is currently a Distinguished Professor of mechanical and aerospace engineering, holds the Alspach Endowed Chair, and is the Founding Director of the Cymer Center for Control Systems and Dynamics, University of California at San Diego (UCSD), La Jolla, CA, USA. He also serves as the Senior Associate Vice Chancellor for research at UCSD. He has coauthored 18 books on adaptive, nonlinear, and stochastic control, extremum seeking, control of PDE systems including turbulent flows, and control of delay

systems.

Prof. Krstić has been elected as a fellow of six scientific societies-IFAC, ASME, SIAM, AAAS, IET (U.K.), and AIAA (Associate Fellow). He has also been elected as a Foreign Member of the Serbian Academy of Sciences and Arts and of the Academy of Engineering of Serbia. As a graduate student, he has received the UC Santa Barbara Best Dissertation Award and the Student Best Paper Awards at CDC and ACC. He has received the Richard E. Bellman Control Heritage Award, the SIAM Reid Prize, the ASME Oldenburger Medal, the Nyquist Lecture Prize, the Paynter Outstanding Investigator Award, the Ragazzini Education Award, the IFAC Ruth Curtain Distributed Parameter Systems Award, the IFAC Nonlinear Control Systems Award, the Chestnut Textbook Prize, the Control Systems Society Distinguished Member Award, the PECASE, NSF Career, and ONR Young Investigator Awards, the Schuck ('96 and '19) and Axelby Paper Prizes, and the First UCSD Research Award given to an engineer. He has also been awarded the Springer Visiting Professorship at University of California at Berkeley, the Distinguished Visiting Fellowship of the Royal Academy of Engineering, the Invitation Fellowship of the Japan Society for the Promotion of Science, and four Honorary Professorships outside of USA. He has served as the Vice President for Technical Activities of the IEEE Control Systems Society and as the Chair for the IEEE CSS Fellow Committee. He serves as the Editor-in-Chief for Systems and Control Letters and has been serving as a Senior Editor for Automatica and IEEE TRANSACTIONS ON AUTOMATIC CONTROL, and an Editor for two Springer book series.